Journal of
Materials Chemistry A

Accepted Manuscript

This article can be cited before page numbers have been issued, to do this please use: K. R. Rao, S. Pishgar, J. Strain, B. KUMAR, V. Atla, S. Kumari and J. Spurgeon, *J. Mater. Chem. A*, 2018, DOI: 10.1039/C7TA09672K.

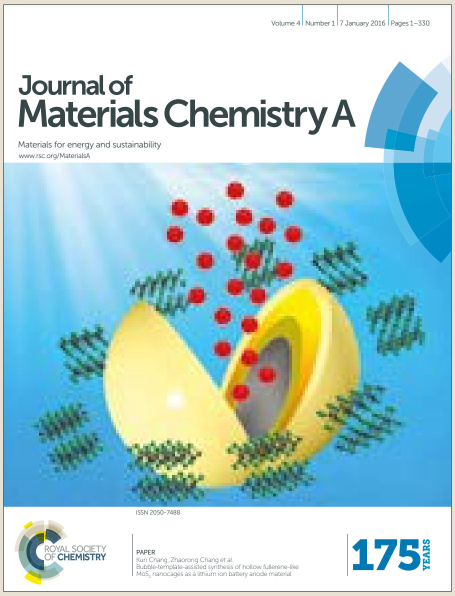

Volume 4 | Number 1 | 7 January 2016 | Pages 1–330

Journal of
Materials Chemistry A

Materials for energy and sustainability
www.rsc.org/MaterialsA

ISSN 2050-7488

ROYAL SOCIETY OF CHEMISTRY

PAPER
Kun Chang, Zhaorong Chang et al.
Bubble-template-assisted synthesis of hollow fullerene-like MoS_2 nanocages as a lithium ion battery anode material

175 YEARS

ROYAL SOCIETY OF CHEMISTRY

rsc.li/materials-a

Journal of Materials Chemistry A

View Article Online
DOI: 10.1039/C7TA09672K

ARTICLE

Photoelectrochemical Reduction of CO_2 to HCOOH on Silicon Photocathodes with Reduced SnO_2 Porous Nanowire Catalysts

Received 00th January 20xx,
Accepted 00th January 20xx

DOI: 10.1039/x0xx00000x

www.rsc.org/

K. Ramachandra Rao,[a,b] Sahar Pishgar,[b] Jacob Strain,[b] Bijandra Kumar,[b,c] Veerendra Atla,[b] Sudesh Kumari,[b] and Joshua M. Spurgeon[b,*]

Electrochemical reduction of CO_2 to liquid products offers a route for the energy-dense storage of intermittent renewable electricity while simultaneously helping to mitigate greenhouse gas emissions. In this work, high-quality Si photocathodes decorated with an earth-abundant Sn porous nanowire catalyst utilized the energy from visible light absorption to provide a photovoltage-assisted conversion of CO_2 to liquid HCOOH. The Sn porous nanowire catalysts were selected for their high density of grain boundaries which was previously shown to enhance activity for formic acid formation. A faradaic efficiency of ~ 60% with a partial current density of 10 mA cm^{-2} for HCOOH was achieved at -0.4 V vs. RHE under illumination, which reflected a positive potential shift of ~ 400 mV compared to the dark electrocatalytic behavior. The photo-assisted electrolysis efficiency for formic acid was calculated to be 11.0%. The results represent a promising photocathode for a narrow bandgap subcell for a tandem photoelectrode system for unbiased light-driven CO_2 electroreduction.

Introduction

Harnessing the energy of sunlight to drive chemical reactions is one of the most promising routes for the storage of intermittent solar energy.[1, 2] The formation of chemical bonds in fuels is a particularly energy-dense storage method, and the liquid products of CO_2 electroreduction with water have a greater volumetric energy density than H_2 from water-splitting. Solar electrochemical CO_2 conversion thus contributes to sustainability as a carbon-neutral, seasonal-length storage technology in which the liquid products can be utilized at night, during off-peak demand periods, or in transportation applications.[3, 4]

Although other liquid products such as ethanol have been produced through CO_2 electroreduction at low to moderate faradaic efficiency,[5-7] much greater selectivity has been achieved for formic acid.[8] Sn and SnO_x foils and nanostructures in particular have been prevalent electrocatalysts for the high faradaic efficiency formation of HCOOH.[9-12] The benefits of HCOOH include stability and low volatility, and it is competitive with current state-of-the-art H_2 storage methods with a viable volumetric capacity of 53.4 g H_2/L at ambient temperature and pressure.[13, 14] HCOOH can also be consumed as a fuel in direct formic acid fuel cells. Moreover, the high market value of HCOOH per CO_2 consumed makes it one of the most economically practical products for the initial establishment of an industrial electrochemical CO_2 reduction process.[15]

In recent years, an increasing effort has been directed towards the realization of solar fuels through photoelectrochemical CO_2 reduction.[16, 17] For photoelectrochemical HCOOH formation in particular, numerous studies have used photoanode materials to drive a separate CO_2 reduction electrocatalyst at the cathode,[18-23] and some have used photocathodes with a co-catalyst.[24-29] With a sophisticated tandem III-V photoanode in combination with a noble metal Pd cathode, up to 10% solar-energy-conversion to formic acid has been achieved.[30] The equilibrium potential for the reduction of CO_2 to formic acid is close to that for hydrogen evolution,[16] and thus high efficiencies should be achievable with two-junction tandem photoelectrodes similar to that modeled for unassisted water-splitting.[31] Si, as a well-developed, low-cost semiconductor with a band gap of 1.12 eV, is a prominent candidate for a bottom subcell photocathode in such a tandem. Photocathodes of p-Si integrated with Cu and Ag catalysts have previously been demonstrated to provide light-enhanced CO_2 reduction, with the resulting faradaic efficiencies and product distribution offset by the Si photovoltage but otherwise largely unchanged.[32]

Recently, we reported electrochemically reduced porous SnO_x nanowire (Sn-pNW) catalysts produced by a highly scalable plasma synthesis.[12] An acid etching step during the catalyst processing was observed to introduce the nanoporosity as well as an increase in crystalline grain boundaries, which resulted in notably enhanced CO_2 reduction current density and faradaic efficiency for HCOOH. The enhanced activity was much greater than could be attributed to increased surface area in the Sn-pNWs alone, and the improved performance was credited to the introduction of more effective active sites at the grain

---

[a] *Crystal Growth and Nano-Science Research Center, Department of Physics, Government College (A), Rajamahendravaram, Andhra Pradesh, India, 533 105.*
[b] *Conn Center for Renewable Energy Research, University of Louisville, Louisville, Kentucky, 40292, USA. *Email - joshua.spurgeon@louisville.edu*
[c] *Department of Technology, Elizabeth City State University, Elizabeth City, NC 27909*

View Article Online
DOI: 10.1039/C7TA09672K

boundaries. Herein we have incorporated these catalysts on Si photocathodes for the photoelectrochemical conversion of CO_2 to HCOOH at high selectivity.

Experimental

Electrode preparation

The synthesis of Sn-pNW catalysts has been described in detail previously.[12, 33] Briefly, a solvo-plasma synthesis method was used in which bulk SnO_2 powder was mixed with KOH in a 3:1 weight ratio and exposed to an atmospheric plasma of Ar and air at 1 kW for 2 min. This process resulted in a potassium-rich (~7%) SnO_2 nanowire (Sn-NW) form which was separated from the larger particles by centrifugation. The as-synthesized Sn-NWs were then immersed in 0.1 M HCl for 1 h to etch the potassium-rich nanowires. The acid etch removed most of the K atoms and produced the porous SnO_2 nanowires (Sn-pNWs) with a high density of grain boundaries.[12] The Sn-pNWs were subsequently calcined in air at 500 °C for 7 h.

Three types of electrode substrate were used throughout the work. Fluorine-doped tin oxide (FTO) coated glass (TEC 15, Hartford Glass Company, Inc.) substrates were used to measure the electrocatalyst properties by itself. Degenerately doped n^+-Si(100) (doped with As to a resistivity of 0.001 – 0.005 Ω cm, University Wafer) substrates were used to measure the dark electrocatalytic behavior of the Si semiconductor surface as well as the Si-supported Sn-pNW electrocatalyst behavior. Photoactive substrates consisted of a buried-junction n^+p-Si wafer (p-Si(100) doped with B to 1 – 10 Ω cm, University Wafer, with n^+ emitter layer from P thermal diffusion to a junction depth of ~ 200 nm following an established procedure[34]). Before drop-casting Sn-pNW catalysts on Si substrates, the Si native oxide layer was removed with a 10 s dip in 10% HF. To load catalyst on the electrodes, 5 mg of Sn-pNWs were sonicated in 1 mL of isopropanol, and then drop-cast onto the substrate in three separate intervals (with 15 min in between for drying) to an approximate loading of ~2 mg cm^{-2}, followed by 2 h on a hot plate at 70 °C. An ohmic back contact to Si substrates was made using Ga/In eutectic (Alfa Aesar).

Photoelectrochemical measurements

Current density vs. potential (*J*-*E*) photoelectrochemical energy-conversion behavior for all electrodes was measured in CO_2-saturated 0.1 M $KHCO_3$ (pH 6.8, made with 18 MΩ cm H_2O) under stirring with active bubbling of CO_2 (99.99%, Specialty Gases) at a flow rate of 10 sccm at room temperature. The FTO or Si electrode served as a working electrode with a Ag/AgCl (saturated KCl) reference electrode (CH Instruments, Inc.) along with a Pt gauze counter electrode separated from the main cell compartment by an anion exchange membrane (Selemion AMV) in a glass cell with a flat quartz window for illumination. Before each measurement with a Si electrode, the native oxide was removed with a 10 s dip in 10% HF. A potentiostat (Bio-Logic SP-200) with electrochemical impedance spectroscopy (EIS) was used for all measurements. Potentiostatic EIS measurements were performed before every experiment to determine the uncompensated solution resistance, R_u, and the potentiostat subsequently compensated for 85% of R_u during electrolysis. The results are reported versus the reversible hydrogen electrode (RHE) scale according to $V_{RHE} = V_{Ag/AgCl} + 0.197 + 0.059*\mathrm{pH}$. Simulated sunlight at an intensity of 100 mW cm^{-2} at normal incidence to the working electrode was generated with a 300 W Xe lamp (Newport 6258) coupled with an AM1.5 global filter (Newport 81094) and calibrated in the electrolyte with a Si photodiode (Thorlabs FDS100-CAL).

Product quantification

CO_2 reduction products were measured by gas chromatography (GC, SRI 8610) for gaseous products and by nuclear magnetic resonance (NMR, Bruker 400 MHz) spectroscopy for liquid products. Both instruments were calibrated with standard gases or liquid solutions. The gas outlet from the catholyte was connected to the GC which used an automatic valve injection (1 mL sample) and a thermal conductivity detector (TCD) and flame ionization detector (FID). Nitrogen (99.99%, Specialty Gases) was used as the carrier gas to enable accurate hydrogen quantification. For potentiostatic conditions at each measured potential, the gas was injected after 5 min and again twice at 18 min intervals. For ^1H NMR spectroscopy analysis of the liquid phase, samples were prepared by mixing D_2O and electrolyte aliquots in a 1:1 volume ratio. Dimethyl sulfoxide (DMSO) was added at a known low concentration for internal calibration. Faradaic efficiency for each product was calculated by determining the charge required to produce the measured product concentration and dividing by the total charge passed during the potentiostatic electrolysis measurement.

Materials characterization

The Sn-pNW catalysts were characterized with scanning electron microscopy (SEM) using a NOVA FEI microscope at an accelerating voltage of ~ 10 – 15 kV and with transmission electron microscopy (TEM) using a Tecnai FEI microscope equipped with a Gatan 2002 GIF system at an accelerating voltage of 200 kV. The samples were prepared by depositing Sn-pNWs on a TEM grid (PELCO Center-Marked Grids) in powder form. An HR XRD Bruker D8 Discover diffractometer was used for X-ray diffraction (XRD) analysis. The XRD operated at 40 kV and 40 mA with Cu Kα (λ = 0.1548 nm) radiation at a scan speed of 6 s per step with a step size of 0.02°. The samples were scanned between 10 - 90° using the θ - 2θ method. EVA software and the Powder Diffraction File were used to analyze the material crystallinity and phases.

Results and discussion

Catalyst characterization

The Sn-pNWs used as a co-catalyst for the photoelectrochemical reduction of CO_2 were characterized via electron microscopy and XRD (Fig. 1). As seen in the SEM of Fig. 1a, the ~ 50 nm diameter, 400 – 700 nm long nanowires were deposited with a dense coverage at the electrode surface. The

View Article Online
DOI: 10.1039/C7TA09672K

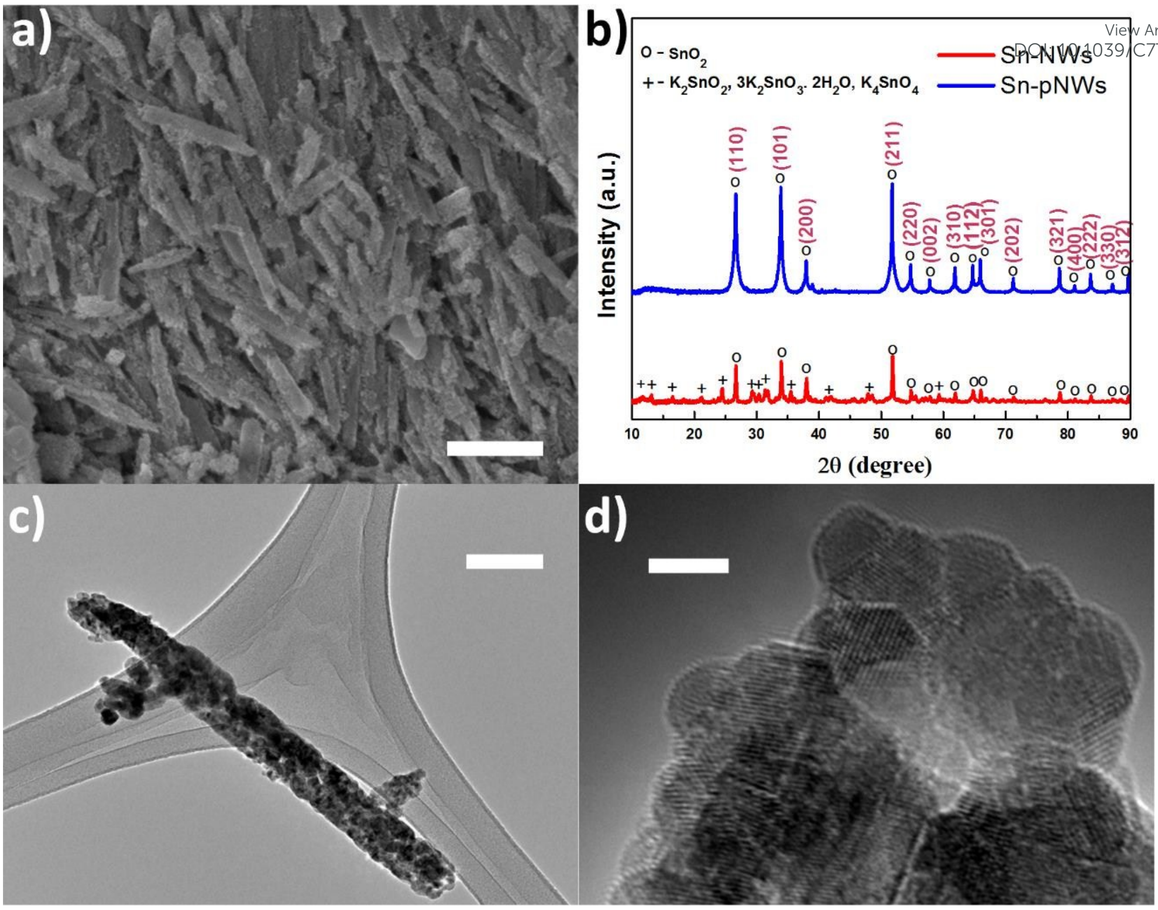

Fig. 1. (a) SEM image of Sn-pNWs drop-cast on a Si substrate, scale bar is 300 nm. (b) XRD data for as-synthesized Sn-NWs before etching, and Sn-pNWs after etching. (c-d) TEM images of a Sn-pNW with (c) scale bar 100 nm, and (d) scale bar 5 nm.

drop-casting deposition process resulted in a film of Sn-pNWs ~ 2 – 3 μm thick across most of the area, however, agglomeration of particles in some spots led to imperfect catalyst layer uniformity (Fig. S1). Before electrochemical reduction of the catalyst oxide during electrolysis, XRD showed a polycrystalline material of the SnO_2 phase (Fig. 1b). The various phases of potassium-tin oxides observed before the acid etch step in the as-synthesized Sn-NWs were absent after the acid etch to form the Sn-pNW material. TEM micrographs of individual Sn-pNW catalysts show the nanoscopic pores throughout the wires (Fig. 1c), and the high-resolution images show the misaligned lattice fringes of nanocrystallite grains, where the interface between each crystallite marks a grain boundary (Fig. 1d).

Photoelectrochemical behavior

The photoelectrochemical CO_2 reduction current density vs. potential (*J*-*E*) behavior of the electrodes are shown in Fig. 2. The dark electrocatalytic performance of Sn-pNWs in the absence of substrate effects from the Si semiconductor was first established on flat FTO/glass substrates. Blank FTO is a kinetically poor surface for the reaction, while the addition of Sn-pNWs led to ~ 10 mA cm^{-2} at -1.0 V vs. RHE (Table 1). At the chosen catalyst loading, this performance was comparable to that previously reported on structured porous carbon gas diffusion layer substrates, which was competitive with many other reported Sn-based CO_2 reduction catalysts.[12]

For Si electrodes, degenerately doped n$^+$-Si substrates were used to measure the dark electrocatalytic properties owing to their metallic character and abundance of majority-carrier electrons available for driving reduction under cathodic conditions. In contrast, for a buried-junction n$^+$p-Si or a photoelectrochemical liquid junction to p-Si, reverse bias conditions for the resulting diode behavior in the dark prevent the flow of electrons across the interface and prohibit the measurement of exponentially increasing current density characteristic of electrocatalytic Butler-Volmer kinetics.[34-37] The degenerate n$^+$-Si substrates were thus used to capture this dark kinetic behavior of the Si surface to enable the photogenerated performance of the buried-junction electrodes to be compared to the dark Si cathodic overpotential behavior. For all Si electrodes, the surface was chemically etched prior to measurement to prevent the ~ 1 – 2 nm native oxide from impeding charge transfer across the Si/water or Si/Sn-pNW

Table 1. Photoelectrochemical energy-conversion parameters.

Electrode	Condition	Onset Potential (V vs. RHE)	Potential @10 mA cm^{-2} (V vs. RHE)
FTO/Sn-pNWs	Dark	-0.36	-1.00
n$^+$-Si	Dark	-0.75	-1.30
n$^+$-Si/Sn-pNWs	Dark	-0.42	-0.98
n$^+$p-Si	1 Sun, AM1.5	-0.15	-0.64
n$^+$p-Si/Sn-pNWs	1 Sun, AM1.5	0.32	-0.25

View Article Online
DOI: 10.1039/C7TA09673K

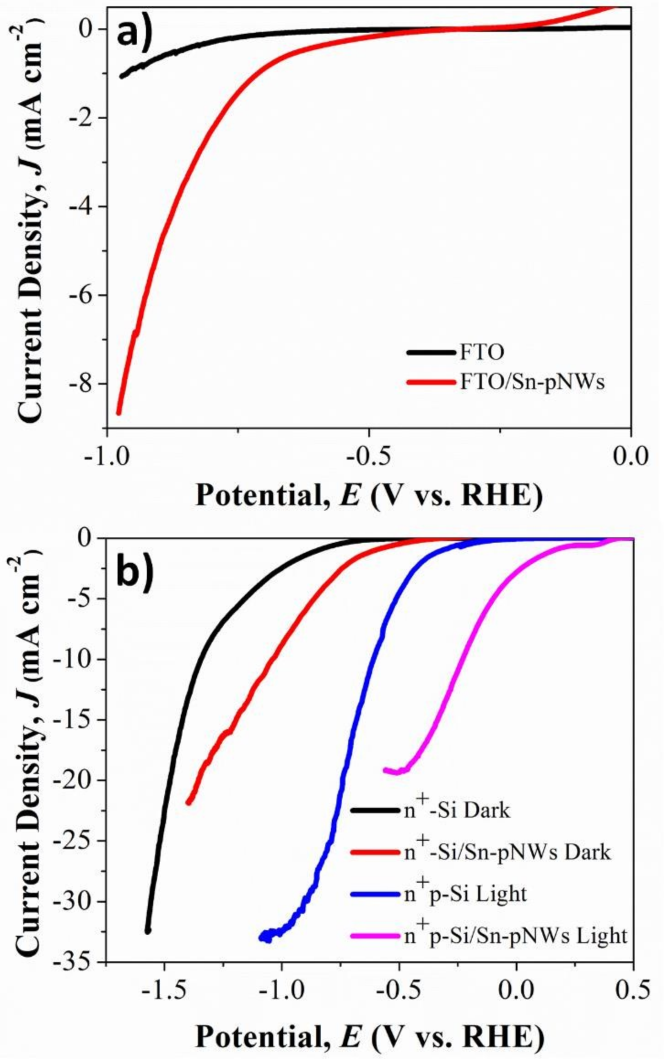

Fig. 2. Current density vs. potential (*J-E*) behavior for electrodes in CO_2-saturated 0.1 M $KHCO_3$. (a) Dark electrocatalytic behavior for FTO/glass with and without Sn-pNW catalyst. (b) Dark electrocatalytic behavior for degenerate n^+-Si with and without Sn-pNW catalyst and illuminated 1 Sun AM1.5 behavior for buried-junction n^+p-Si photocathodes with and without Sn-pNW catalyst.

interface. In the dark, bare n^+-Si electrodes exhibited a cathodic current onset at ~ -0.75 V vs. RHE and reached 10 mA cm^{-2} at -1.30 V vs. RHE. With the addition of Sn-pNW co-catalyst, the cathodic current onset increased to ~ -0.42 V vs. RHE and reached 10 mA cm^{-2} at -0.98 V vs. RHE, a decrease of ~ 320 mV in overpotential compared to the bare Si. However, the resulting linear ohmic character of the *J-E* curve for dark n^+-Si/Sn-pNWs indicates an appreciable increase in series resistance, which we attribute to the interfacial series resistance from the contiguous Sn-pNW layer (Fig. 1a). If it was directly contacting a p-Si photocathode, this unbroken layer of Sn-pNWs would establish the barrier height at the Sn/Si interface and restrict the achievable photovoltage in a liquid-junction photoelectrochemical cell.[34, 38] By using a buried-junction n^+p-Si photoelectrode instead, the Si homojunction can maintain maximum photovoltage with minimal recombination at the junction interface.[34, 39] Charge-transfer resistance at the Si/Sn-pNW interface may also contribute to the increased ohmic overpotential. However, the SnO_2 conduction band edge is significantly lower (i.e., more positive) than the Si conduction band edge,[40] which should promote photoexcited electron transfer to the co-catalyst for photoelectrochemical CO_2 reduction.

The bare buried-junction n^+p-Si photoelectrode under 1 Sun AM1.5 illumination showed the expected behavior relative to the bare n^+-Si. Illuminated bare n^+p-Si exhibited an onset for cathodic current at ~ - 0.15 V vs. RHE, achieving 10 mA cm^{-2} at -0.64 V vs. RHE, and reaching a light-limited current density of ~ 33.0 mA cm^{-2}. Coating the n^+p-Si with Sn-pNW co-catalyst, the onset potential shifted to ~ 0.32 V vs. RHE and exhibited 10 mA cm^{-2} at -0.25 V vs. RHE. The illuminated n^+p-Si/Sn-pNWs photoelectrodes displayed a reduced light-limited current density (~ 19.5 mA cm^{-2}) relative to the bare photoelectrodes due to parasitic light absorption within the Sn-pNW co-catalyst layer. The reduced photocurrent was consistent with the measured catalyst layer transmittance which averaged ~ 60% at wavelengths above the Si bandgap (Fig. S4). The n^+p-Si/Sn-pNWs electrode also maintained > 90% of its photocurrent after > 3 h of operation (Fig. S5). On illuminated buried-junction n^+p-Si photoelectrodes at 10 mA cm^{-2}, the Sn-pNW catalyst thus decreased the overpotential by ~ 390 mV. Moreover, the positive shift in potential at 10 mA cm^{-2} from dark Si electrocatalytic behavior to the illuminated performance reflects a 1-Sun generated photovoltage of ~ 660 mV for the n^+p-Si. This is a high photovoltage for Si, indicating a quality junction and low overall recombination. For Sn-pNW catalyzed electrodes, the light-driven positive shift in potential at 10 mA cm^{-2} was even greater at 730 mV. This shift is perhaps too large to attribute to a buried-junction Si photovoltage alone, and we attribute the remainder to a slightly better catalyst interface with less series resistance compared to the dark n^+-Si/Sn-pNW electrode.

CO_2 reduction product distribution

The faradaic efficiencies for CO_2 reduction products measured at the cathode are shown in Fig. 3a for FTO/Sn-pNWs in the dark and for n^+p-Si/Sn-pNWs under 1-Sun illumination. The only products observed at these conditions by GC were H_2 and CO, and the only liquid product observed by NMR was HCOOH. At low applied potential (> -0.4 V vs. RHE) in the dark on FTO, H_2 was the dominant product with > 95% faradaic efficiency. However, the selectivity for formic acid increased greatly at more cathodic potentials, reaching as high as 65.9% at -0.8 V vs. RHE, consistent with previously reported results on porous carbon electrodes.[12] The CO faradaic efficiency for FTO/Sn-pNWs at this potential was limited to 9.2%. The same trend in product distribution was observed under illumination on n^+p-Si/Sn-pNWs with H_2 being the sole product detected at potentials > -0.1 V vs. RHE, while the peak HCOOH faradaic efficiency was 59.2% at -0.4 V vs. RHE with a corresponding CO faradaic efficiency of 11.4%. Although the light-driven positive potential shift was less than observed in the *J-E* curves, the overpotential for peak formic acid selectivity decreased by at least 400 mV. The energy of the incident light was thus converted to assist in the reduction of CO_2 to a useful liquid product as HCOOH. Without the Sn-pNW catalyst, n^+p-Si electrodes produced primarily H_2 with < 10% faradaic efficiency for CO (Fig. S6).

The partial current density of each product is displayed in Fig. 3b for illuminated n^+p-Si/Sn-pNW photoelectrodes. The partial current density of formic acid, J_{HCOOH}, achieved 10.0 mA cm^{-2} at -0.4 V vs. RHE, increasing only slightly at more negative potentials as the photoelectrode reached its light-limited current density. For dark FTO/Sn-pNWs at -0.8 V vs. RHE, the potential measured for peak HCOOH faradaic efficiency, J_{HCOOH} was only 1.64 mA cm^{-2}. Only some of the best literature Sn-based catalysts have reported $J_{HCOOH} \geq 10$ mA cm^{-2}. For instance, SnO_x on graphene was reported to produce J_{HCOOH} ~ 10 mA cm^{-2} at -1.15 V vs. RHE.[10] Hierarchical mesoporous SnO_2 nanosheets on carbon cloth are among the highest current density formic-acid-selective CO_2 electroreduction systems reported to date, but they required a cathodic potential of at least -0.8 V vs. RHE to achieve $J_{HCOOH} \geq 10$ mA cm^{-2}.[41] Thus a solar-driven J_{HCOOH} ~ 10 mA cm^{-2} at -0.4 V vs. RHE makes this Si photoelectrode quite competitive for Sn-catalyzed HCOOH electrosynthesis from CO_2.

To estimate the system efficiency for the photoelectrochemical energy-conversion behavior of the illuminated n^+p-Si/Sn-pNW photoelectrode for CO_2 reduction, a photo-assisted electrolysis system efficiency, η_{PAE}, was calculated by:[42]

$$\eta_{PAE} = \frac{P_{f,o}}{P_s + P_{e,i}}$$

where $P_{f,o}$ is the output power density contained in the chemical fuel produced, P_s is the incident illumination power density, and $P_{e,i}$ is the input electrical power density. Considering the energy stored in the multiple products of this system (H_2, CO, HCOOH):

$$\eta_{PAE} = \frac{J_{op}\left(\varepsilon_{H2}E_{f,H2} + \varepsilon_{CO}E_{f,CO} + \varepsilon_{HCOOH}E_{f,HCOOH}\right)}{P_s + J_{op}V_{e,i}}$$

where J_{op} is the operating current density at the potential under evalution, ε_i represents the faradaic efficiency of each respective product, $E_{f,i}$ is the potential difference corresponding to the Gibbs free-energy difference between the two half-reactions of the fuels being produced, and $V_{e,i}$ is the input voltage required to drive the electrolysis at the operating current density of interest. $V_{e,i}$ is the total applied bias to the system, and thus represents the voltage required in a two-electrode electrolysis measurement. However, by separately measuring the *J-E* behavior of the Pt gauze anode in the cell, the corresponding anodic overpotential at J_{op} can be accounted for to estimate $V_{e,i}$.[42] In the current system for n^+p-Si/Sn-pNWs under illumination at -0.4 V vs. RHE, $V_{e,i}$ was estimated to be ~ 2.03 V. Using literature values for the cathodic half-reaction potentials for each product,[43] we determined the total η_{PAE} ~ 17.4%. For the formic acid product alone, $\eta_{PAE,HCOOH}$ ~ 11.0%. Though informative, photo-assisted electrolysis efficiency should not be compared directly with solar-to-fuel efficiency in the absence of electrical bias since electricity-to-fuel efficiency is typically much higher than solar-energy-conversion efficiency.[42] To produce HCOOH with the n^+p-Si/Sn-pNWs photocathode from sunlight unassisted by electrical bias, extra series-connected solar cells or a tandem combination with complementary bandgap subcells would be required to achieve the necessary additional photovoltage.

View Article Online
DOI: 10.1039/C7TA09672K

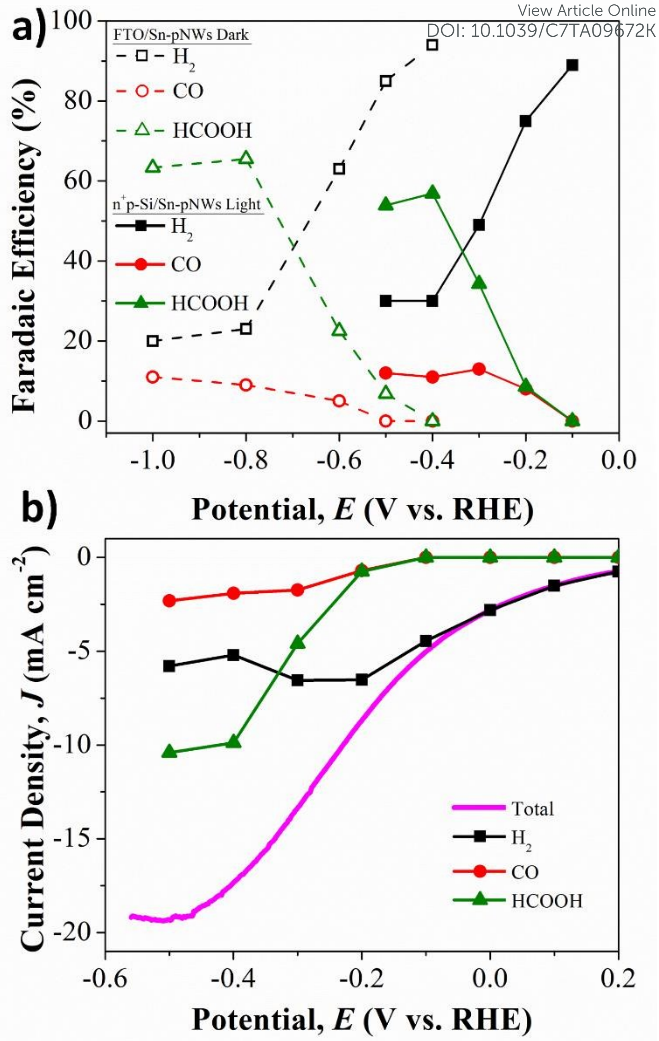

Fig. 3. CO_2 reduction product distribution in CO_2-saturated 0.1 M $KHCO_3$. (a) Faradaic efficiency for H_2 (squares), CO (circles), and HCOOH (triangles) for FTO/Sn-pNWs in the dark (dashed lines, open markers) and for n^+p-Si/Sn-pNWs under 1 Sun AM1.5 illumination (solid lines, filled markers). (b) The current density vs. potential for illuminated n^+p-Si/Sn-pNWs and corresponding partial current density for the reaction products.

Conclusions

High-quality Si photocathodes coupled with porous tin oxide nanowire co-catalyst with a high density of grain boundaries were used to harness the energy of visible light to assist in the conversion of CO_2 to formic acid. The buried-junction n^+p-Si interface permitted a contiguous layer of Sn-pNW catalyst at the interface without limiting the effective barrier height and corresponding photovoltage. The electrons from the cathode were thus able to utilize the added potential from the photogenerated quasi-Fermi-level splitting in the illuminated Si to drive the CO_2 reduction half-reaction at lower applied

View Article Online
DOI: 10.1039/C7TA09672K

potentials than in the dark without significantly altering the product distribution. The potential for peak faradaic efficiency of HCOOH was observed to shift ~ 400 mV under illumination, with Si photocathodes achieving a faradaic efficiency of 59.2% at -0.4 V vs. RHE and a partial current density for formic acid formation of J_{HCOOH} ~ 10 mA cm^{-2}. As an energy-dense liquid product with a high profit margin relative to other CO_2 reduction products, formic acid is appealing as a molecule for the storage of intermittent solar energy. The demonstrated photocathodes could thus serve as one component of a tandem system for a viable solar-driven CO_2-to-HCOOH process.

Conflicts of interest

There are no conflicts to declare.

Acknowledgements

The authors acknowledge support from the Conn Center for Renewable Energy Research at the University of Louisville. K.R. Rao also acknowledges support from the University Grants Commission, Government of India, for providing a Raman Post-doctoral Fellowship to conduct work at the Conn Center at the University of Louisville. We also gratefully acknowledge assistance from Dr. Jacek Jasinski of the Materials Characterization Service Center of the Conn Center at the University of Louisville.

Notes and references

1. N. S. Lewis and D. G. Nocera, *Proc. Natl. Acad. Sci. U. S. A.*, 2006, **103**, 15729-15735.
2. M. Gratzel, *Philos. Trans. R. Soc. A-Math. Phys. Eng. Sci.*, 2007, **365**, 993-1005.
3. M. Mikkelsen, M. Jorgensen and F. C. Krebs, *Energy Environ. Sci.*, 2010, **3**, 43-81.
4. S. C. Roy, O. K. Varghese, M. Paulose and C. A. Grimes, *ACS Nano*, 2010, **4**, 1259-1278.
5. T. T. H. Hoang, S. C. Ma, J. I. Gold, P. J. A. Kenis and A. A. Gewirth, *ACS Catal.*, 2017, **7**, 3313-3321.
6. Y. Hori, I. Takahashi, O. Koga and N. Hoshi, *Journal of Molecular Catalysis a-Chemical*, 2003, **199**, 39-47.
7. D. Ren, B. S. H. Ang and B. S. Yeo, *ACS Catal.*, 2016, **6**, 8239-8247.
8. J. Qiao, Y. Liu, F. Hong and J. Zhang, *Chem. Soc. Rev.*, 2014, **43**, 631-675.
9. Y. H. Chen and M. W. Kanan, *J. Am. Chem. Soc.*, 2012, **134**, 1986-1989.
10. S. Zhang, P. Kang and T. J. Meyer, *J. Am. Chem. Soc.*, 2014, **136**, 1734-1737.
11. M. F. Baruch, J. E. Pander, J. L. White and A. B. Bocarsly, *ACS Catal.*, 2015, **5**, 3148-3156.
12. B. Kumar, V. Atla, J. P. Brian, S. Kumari, T. Q. Nguyen, M. Sunkara and J. M. Spurgeon, *Angew. Chem.-Int. Edit.*, 2017, **56**, 3645-3649.
13. D. Mellmann, P. Sponholz, H. Junge and M. Beller, *Chem. Soc. Rev.*, 2016, **45**, 3954-3988.
14. A. K. Singh, S. Singh and A. Kumar, *Catalysis Science & Technology*, 2016, **6**, 12-40.
15. S. Verma, B. Kim, H. Jhong, S. C. Ma and P. J. A. Kenis, *Chemsuschem*, 2016, **9**, 1972-1979.
16. B. Kumar, M. Llorente, J. Froehlich, T. Dang, A. Sathrum and C. P. Kubiak, *Annual Review of Physical Chemistry, Vol 63*, 2012, **63**, 541-569.
17. S. Das and W. Daud, *Rsc Advances*, 2014, **4**, 20856-20893.
18. W. W. Lu, B. Jia, B. L. Cui, Y. Zhang, K. S. Yao, Y. L. Zhao and J. J. Wang, *Angew. Chem.-Int. Edit.*, 2017, **56**, 11851-11854.
19. Y. C. Wang, B. AlOtaibi, F. A. Chowdhury, S. Z. Fan, M. G. Kibria, L. Li, C. J. Li and Z. T. Mi, *APL Materials*, 2015, **3**, 116106.
20. Y. H. Yang, R. R. Xie, H. Li, C. J. Liu, W. H. Liu and F. Q. Zhan, *Transactions of Nonferrous Metals Society of China*, 2016, **26**, 2390-2396.
21. Y. H. Yang, F. Q. Zhan, H. Li, W. H. Liu and S. Yu, *J. Solid State Electrochem.*, 2017, **21**, 2231-2240.
22. J. K. Sheu, P. H. Liao, T. C. Huang, K. J. Chiang, W. C. Lai and M. L. Lee, *Sol. Energy Mater. Sol. Cells*, 2017, **166**, 86-90.
23. G. Yin, H. Abe, R. Kodiyath, S. Ueda, N. Srinivasan, A. Yamaguchi and M. Miyauchi, *Journal of Materials Chemistry A*, 2017, **5**, 12113-12119.
24. T. Arai, S. Tajima, S. Sato, K. Uemura, T. Morikawa and T. Kajino, *Chem. Commun.*, 2011, **47**, 12664-12666.
25. X. F. Huang, T. C. Cao, M. C. Liu and G. H. Zhao, *J. Phys. Chem. C*, 2013, **117**, 26432-26440.
26. U. Kang, S. K. Choi, D. J. Ham, S. M. Ji, W. Choi, D. S. Han, A. Abdel-Wahabe and H. Park, *Energy Environ. Sci.*, 2015, **8**, 2638-2643.
27. D. H. Won, C. H. Choi, J. Chung and S. I. Woo, *Applied Catalysis B-Environmental*, 2014, **158**, 217-223.
28. D. H. Won, J. Chung, S. H. Park, E. H. Kim and S. I. Woo, *Journal of Materials Chemistry A*, 2015, **3**, 1089-1095.
29. S. K. Choi, U. Kang, S. Lee, D. J. Ham, S. M. Ji and H. Park, *Advanced Energy Materials*, 2014, **4**, 1301614.
30. X. H. Zhou, R. Liu, K. Sun, Y. K. Chen, E. Verlage, S. A. Francis, N. S. Lewis and C. X. Xiang, *Acs Energy Letters*, 2016, **1**, 764-770.
31. S. Hu, C. X. Xiang, S. Haussener, A. D. Berger and N. S. Lewis, *Energy Environ. Sci.*, 2013, **6**, 2984-2993.
32. R. Hinogami, Y. Nakamura, S. Yae and Y. Nakato, *J. Phys. Chem. B*, 1998, **102**, 974-980.
33. T. Q. Nguyen, V. Atla, V. K. Vendra, A. K. Thapa, J. B. Jasinski, T. L. Druffel and M. K. Sunkara, *Chem. Eng. Sci.*, 2016, **154**, 20-26.
34. S. W. Boettcher, E. L. Warren, M. C. Putnam, E. A. Santori, D. Turner-Evans, M. D. Kelzenberg, M. G. Walter, J. R. McKone, B. S. Brunschwig, H. A. Atwater and N. S. Lewis, *J. Am. Chem. Soc.*, 2011, **133**, 1216-1219.
35. N. C. Strandwitz, D. J. Comstock, R. L. Grimm, A. C. Nichols-Nielander, J. Elam and N. S. Lewis, *J. Phys. Chem. C*, 2013, **117**, 4931-4936.
36. M. X. Tan, P. E. Laibinis, S. T. Nguyen, J. M. Kesselman, C. E. Stanton and N. S. Lewis, in *Progress in Inorganic Chemistry, Vol 41*, 1994, pp. 21-144.
37. A. J. Bard and L. R. Faulkner, *Electrochemical Methods: Fundamentals and Applications*, John Wiley & Sons, 2001.
38. R. C. Rossi, M. X. Tan and N. S. Lewis, *Appl. Phys. Lett.*, 2000, **77**, 2698-2700.
39. M. G. Walter, E. L. Warren, J. R. McKone, S. W. Boettcher, Q. X. Mi, E. A. Santori and N. S. Lewis, *Chem. Rev.*, 2010, **110**, 6446-6473.
40. S. Y. Chen and L. W. Wang, *Chem. Mater.*, 2012, **24**, 3659-3666.
41. F. W. Li, L. Chen, G. P. Knowles, D. R. MacFarlane and J. Zhang, *Angew. Chem.-Int. Edit.*, 2017, **56**, 505-509.

View Article Online
DOI: 10.1039/C7TA09672K

42. R. H. Coridan, A. C. Nielander, S. A. Francis, M. T. McDowell, V. Dix, S. M. Chatman and N. S. Lewis, *Energy Environ. Sci.*, 2015, **8**, 2886-2901.
43. B. Kumar, J. P. Brian, V. Atla, S. Kumari, K. A. Bertram, R. T. White and J. Spurgeon, *Catal. Today*, 2016, **270**, 19-30.

View Article Online
DOI: 10.1039/C7TA09672K

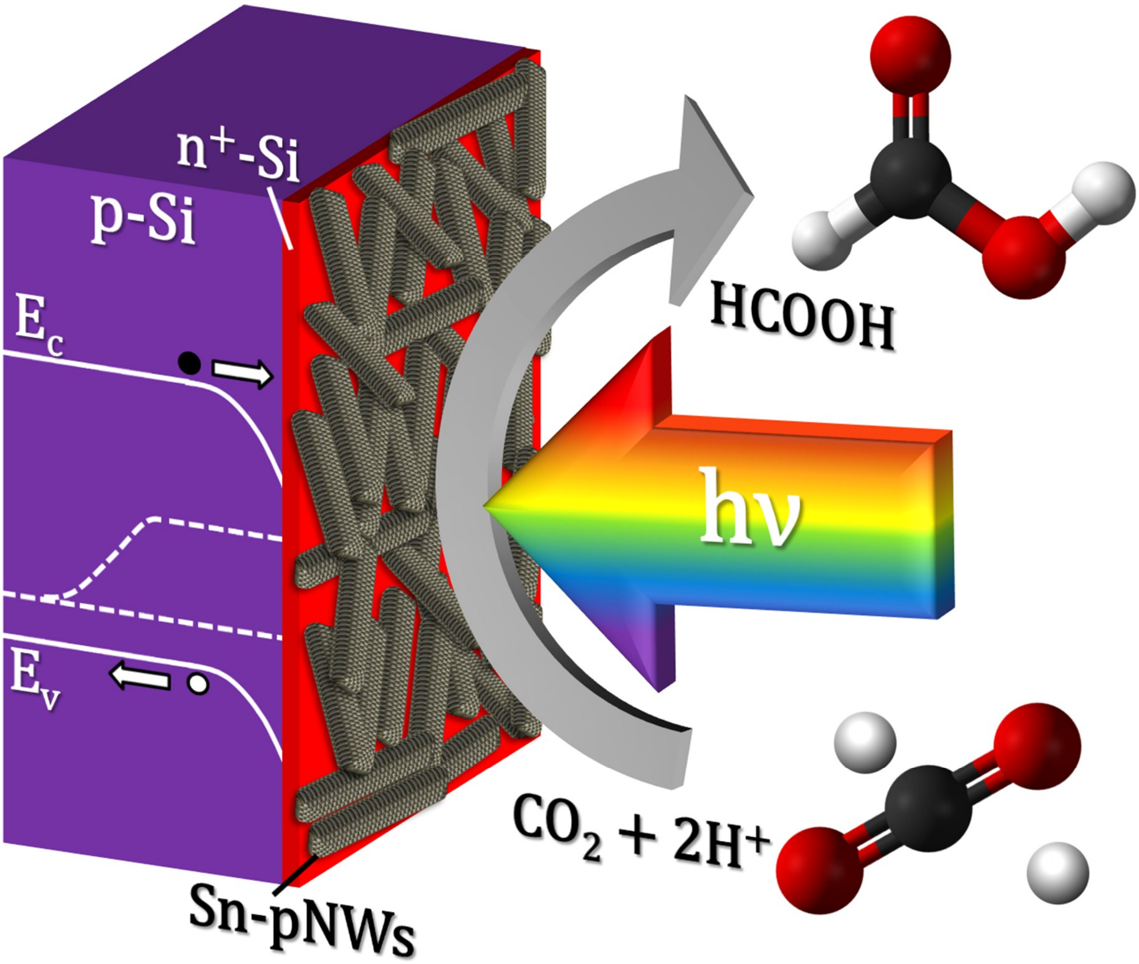

Full Size

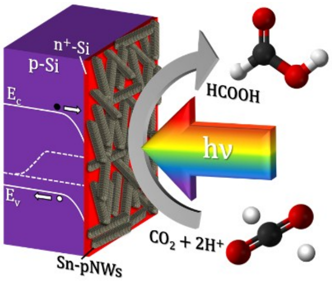

4 cm Height

Caption:
High-quality Si photoelectrodes with novel Sn nanowire catalysts convert solar energy to reduce CO_2 to formic acid with high selectivity.